Korean J. Chem. Eng., 40(12), 3059-3067 (2023)
DOI: 10.1007/s11814-023-1538-4

pISSN: 0256-1115
eISSN: 1975-7220

The electrocatalysis of Mn-Co_3O_4/CeO_2@C particles with different Ce content modified Ti/PbO_2 anode and its application for copper electrodeposition

Zihang Yin*,‡, Ruibo He*,‡, Fei Nie*,†, Zhen Wei, Bo Jia**, Qing Feng**, Xiaolong Fu***, and Wenyan Zhang*,†**

*Key Laboratory of Synthetic and Natural Functional Molecule Chemistry (Ministry of Education), College of Chemistry & Materials Science, Northwest University, Xi'an, 710069, P. R. China
**Xi'an TaiJin Industrial Electrochemical Technology CO., Ltd, Xi'an 710016, China
***Xi'an Modern Chemistry Research Institute, Xi'an 710062, P. R. China
(*Received 16 April 2023 • Revised 15 July 2023 • Accepted 21 July 2023*)

Abstract−The oxygen evolution kinetics of industrial copper electrodeposition is slow, resulting in low electrocatalytic activity and high energy consumption. In this work, a quaternary composite of carbon coated active particles containing Mn, Co and Ce were prepared (Mn-Co_3O_4/CeO_2@C), and Ti/Sb-SnO_2/PbO_2 electrode doped with these active particles was prepared by co-electrodeposition. The microstructure and chemical composition of the electrode was characterized by scanning electron microscopy (SEM), energy dispersive spectroscopy (EDS) and X-ray diffractometry (XRD). Linear sweep voltammetry (LSV), electrochemical impedance spectroscopy (EIS) and Tafel polarization curve (Tafel) were used to study the electrochemical properties of anode materials. The results showed that the doping of Mn-Co_3O_4/CeO_2@C active particles promoted the crystal transition of PbO_2, decreased the average grain size, and the doping of Ce increases the average valence state of Co. The modified titanium electrode showed excellent catalytic activity of the oxygen evolution reaction (OER) characteristics. The overpotential of the doped Ti/Sb-SnO_2/PbO_2 anode was only 453 mV when the current density was 20 mA cm^{-2} in 0.5 M H_2SO_4 solution, which is 508 mV lower than that of the undoped Ti/Sb-SnO_2/PbO_2 anode. In simulated copper electro-deposition experiments, the cell voltage was reduced by about 400 mV, compared to the undoped Ti/Sb-SnO_2/PbO_2 electrode.

Keywords: Titanium Anode, Electrocatalysis, Oxygen Evolution Reaction, Mn-Co_3O_4/CeO_2@C, Copper Electrodeposition

INTRODUCTION

Copper hydrometallurgy plays an increasingly important role in copper smelting because of its advantages of low pollution, low cost and high copper purity. Electrolytic refining is necessary to increase the purity of copper to 99.9 percent or even more [1,2]. In the two electrochemical semi-reaction processes of electrolytic copper, the oxygen evolution reaction (OER) on the anode requires higher overpotential leading to higher energy consumption of electrodeposition copper and accounting for about 30% of the energy consumption of the whole electrolytic process [3]. At present, Pb-Ca-Sn alloy anodes are commonly used for copper electrodeposition due to their low cost, high conductivity and easy machining. However, as the anode in electrolysis, this alloy material is easily corroded by oxidation, resulting in anode slime precipitation.

Since Beer developed the Ti-based dimensionally stable anode (DSA) in the 1960s, much research has been done on DSA anode. Because the DSA electrode has high corrosion resistance and long life, it has been widely used in electroplating, smelting, chlor-alkali industry and wastewater treatment and other fields [4-7]. The substrate of DSA anode has poor electrocatalytic activity, and it is usually necessary to add a catalytic active layer on its surface. Noble metal-based catalysts, such as IrO_2, are ideal for active layer materials because of their high catalytic oxygen evolution activity and stability under acidic conditions [8]. But the high price of iridium, the rarest of the precious metals, has prompted a search for cheaper alternatives. Co_3O_4 has been considered as an ideal alternative material because it has been shown to be active against OER both theoretically and experimentally [9,10]. Unfortunately, Co_3O_4 has poor stability under acidic conditions and cannot remain active for a long time. A recent study has shown that Mn doping can improve the stability of Co_3O_4 under acidic conditions [11].

Ti base lead dioxide (Ti/PbO_2) anode, as an insoluble metal oxide anode material, has been widely studied and applied in hydrometallurgy due to its advantages of simple preparation, low cost, good electrical conductivity and corrosion resistance [12-15]. It is worth noting that PbO_2 has a high overpotential when being used as the anode of OER reaction and resulting in energy loss. To reduce oxygen evolution overpotential, ion or particle doping in PbO_2 is considered to be effective, such as doping Ag^+ [16], Co^{2+} [3], Mn^{2+} [17], Co_3O_4 [18], CeO_2 [19], $MnCo_2O_4$ [20], Mn_2O_3 [21], $MnCo_2O_{4.5}$@C [22] to improve the electrocatalytic activity of PbO_2 anode. Despite considerable effort in the design and manufacture of energy-saving PbO_2 electrodes for copper electrodeposition, there is still room

†To whom correspondence should be addressed.
E-mail: niefei@nwu.edu.cn, wyZhang@nwu.edu.cn
‡These authors contributed equally to this work and should be considered co-first authors.

for improvement. The effect mechanism of various doping elements on the electrocatalytic activity of modified electrode remains to be studied. In particular, the synergistic mechanism between doping of non-electrocatalytic active elements and catalytic activity of electrocatalytic active elements remains unclear. Moreover, an intermediate layer is usually required to improve the poor adhesion of the PbO_2 coating to the Ti matrix [23,24].

In this study, a quaternary composite of carbon coated active particles containing Mn, Co and Ce ($Mn\text{-}Co_3O_4/CeO_2@C$) was synthesized by pyrolysis annealing, and then used to modify the Ti/PbO_2 electrode through co-electrodeposition. The morphological characterization and the electrochemical performance of the undoped and doped Ti/PbO_2 electrodes were compared. Due to the change of surface structure and the increase of intrinsic catalytic activity, the doped Ti/Sb-SnO_2/PbO_2 electrode has the improved catalytic performance of OER. In 0.5 M H_2SO_4 solution, the overpotential of the modified titanium anode is only 453 mV when the current density is 20 mA cm^{-2}. In simulated copper electrodeposition experiments, the use of Ti/Sb-SnO_2/PbO_2 electrodes as the anode reduced the cell voltage by about 400 mV compared to undoped Ti/PbO_2 anode cells. The doped Ti/Sb-SnO_2/PbO_2 electrode has a long service life, operating for about 73 h at a high current density of 20,000 A m^{-2} in 0.5 M H_2SO_4 solution. This study is helpful in preparing high performance modified PbO_2 electrode and plays an active role in reducing production energy consumption in industrial applications.

EXPERIMENTAL SECTION

1. Materials

Cobalt nitrate hexahydrate ($Co(NO_3)_2{\cdot}6H_2O$), Manganese nitrate tetrahydrate ($Mn(NO_3)_2{\cdot}4H_2O$), Cerium nitrate hexahydrate ($Ce(NO_3)_3{\cdot}6H_2O$) copper sulfate pentahydrate ($Cu(NO_3)_2{\cdot}6H_2O$) were supplied by Shanghai Aladdin Biochemical Technology Co., Ltd. Polyvinylpyrrolidone (PVP, K30), lead nitrate ($Pb(NO_3)_2$), concentrated sulfuric acid (H_2SO_4) and concentrated nitric acid (HNO_3) were purchased from Sinopharm Chemical Reagent Co., LTD. The reagents used in this study were all analytically pure (AR).

2. Instrument

The diffraction analysis of the composite anode was carried out using the D8 Advance X-ray powder diffractometer (Bruker Ag, Germany). The structure and chemical composition of the composite anode were studied with SU8010 scanning electron microscope (Hitachi) combined with energy dispersive spectrometer (EDS) spectrum. Linear sweep voltammetry (LSV), Tafel curve and electrochemical impedance spectroscopy (EIS) were measured on CHI660E electrochemical workstation (Shanghai Chenhua Co., LTD). The tests were performed in a standard three-electrode system. The working electrode is a self-made electrode (1 cm×1 cm), and the auxiliary electrode is a platinum electrode (1 cm×1 cm). The reference electrode is a mercurous sulfate electrode (MSE) [25]. In 0.5 M H_2SO_4, EIS test was performed at stable oxygen evolution potential with current density of 10 mA cm^{-2}.

3. Preparation of Sb-SnO_2 Intermediate Layer

An industrial pure titanium sheet (thickness of about 1 mm) was used as the matrix after the surface was polished, etching in 5% sodium hydroxide for 30 min at 25 °C and 6% oxalic acid solution for 2 h at 200 °C, successively. After that, the titanium sheet was rinsed with distilled water and placed in anhydrous ethanol for reserve. $SnCl_4$ and $SbCl_3$ were dissolved in n-butanol, and a small amount of concentrated HCl was added for hydrolysis (the ratio of Sn to Sb was 10 : 1) to prepare the precursor solution. The prepared coating solution was evenly coated on the surface of the treated titanium plate with a fine brush, dried at 60 °C for 10 min, and then transferred to Muffle furnace for sintering at 450 °C for 15 min.

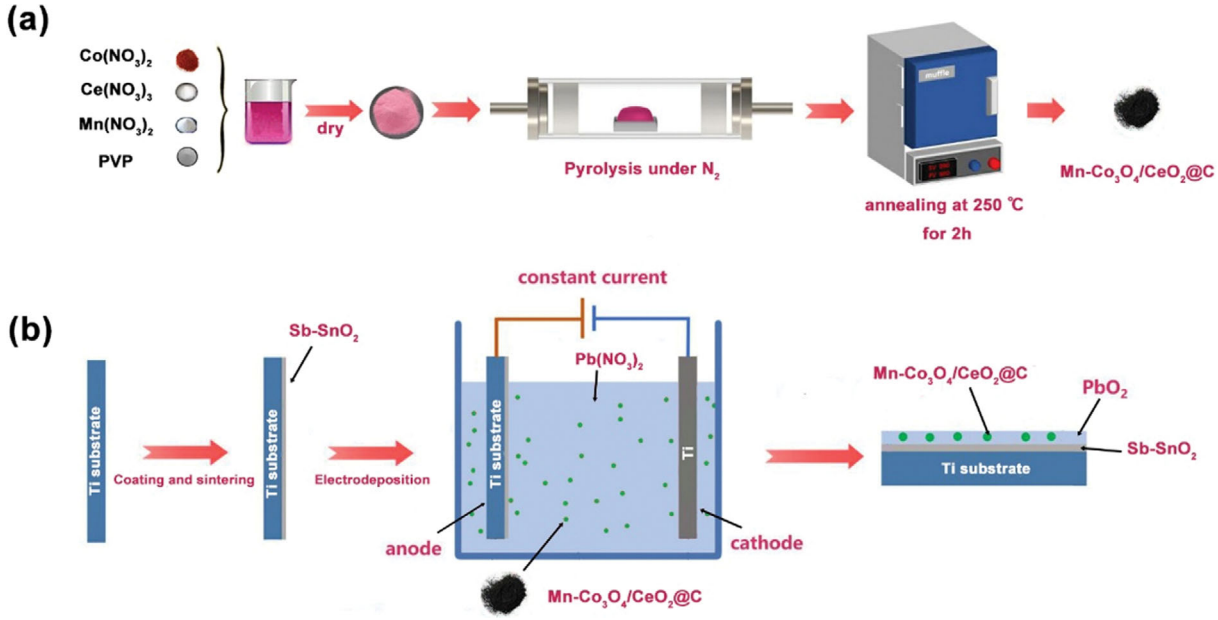

Fig. 1. Schematic diagram of electrode preparation process: (a) preparation of active particles, (b) preparation of intermediate layer and active layer.

4. Preparation of Carbon Coated Active Particles (Mn-Co_3O_4/CeO_2@C)

A series of carbon coated active particles with different components were prepared by pyrolysis annealing. Typically, 3.710 g $Co(NO_3)_2{\cdot}6H_2O$, 0.178 g $Mn(NO_3)_2$, 0.307 g $Ce(NO)_3$ (5% Mn, 15% Ce) and 3 g PVP were dissolved in 40 ml of ethanol to form a uniform solution, which was dried in a 60 °C oven for 24 h to obtain a pink solid. The powder was then pyrolyzed at 600 °C in a tubular furnace under N_2 atmosphere at a heating rate of 7.5 °C/min. Finally, the resulting black powder was further oxidized at 250 °C for 2 h.

5. Preparation of Ti/Sb-SnO_2/PbO_2 Electrodes Modified by Active Particles

The anodic co-deposition method was used to prepare the carbon-coated active particles doped PbO_2 layer. In the electrolyte containing 0.8 M $Pb(NO_3)_2$, 0.02 M HNO_3, and 4 g/L carbon-coated active particles, electrodeposition was carried out for 60 min by constant-current method with a current density of 30 mA cm^{-2}.

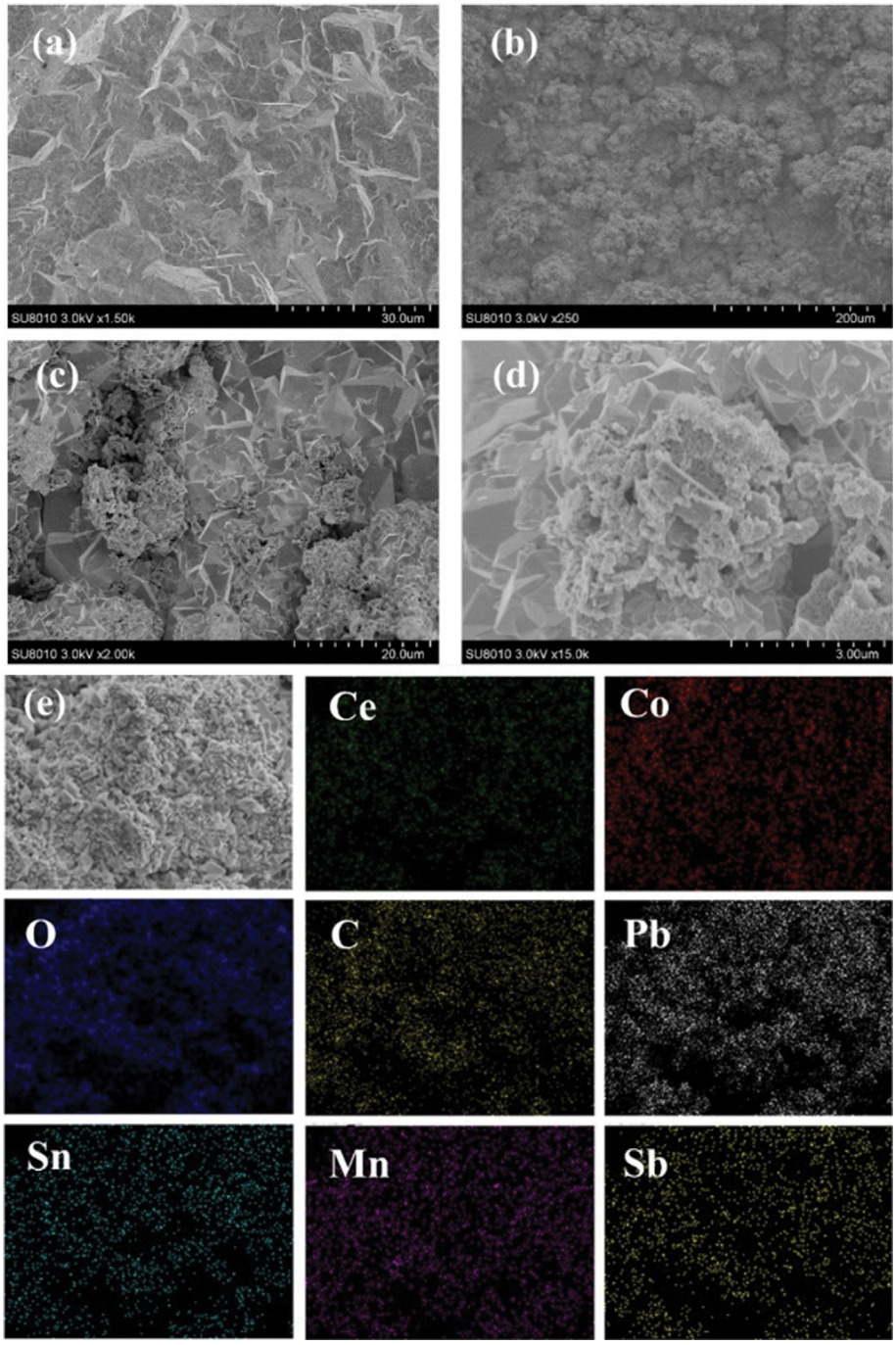

Fig. 2. SEM of electrode surface: (a) Ti/Sb-SnO_2/PbO_2, (b)-(d) Doped Ti/Sb-SnO_2/PbO_2 at different magnifications, (e) EDS for doped Ti/Sb-SnO_2/PbO_2.

The electrolyte was continuously stirred during the electrodeposition process at a constant temperature of 40 °C. The preparation process of active material and anode is shown in Fig. 1.

6. Simulated Copper Electrodeposition

The cell voltage was measured and compared in a simulated electrodeposited copper solution (H_2SO_4 180 g/L, $CuSO_4$ 45 g/L). The anodes were Ti/Sb-SnO_2/PbO_2 doped with and without active particles. The cathode was made of pure titanium plate. The electrolyzation was performed in copper sulfate solution with a current density of 20 mA cm^{-2} for 12 h at 65 °C and the cell voltage was recorded every 30 min.

7. Accelerated Life Time Test

Accelerated life tests were carried out in 0.5 M sulfuric acid solution. Ti/Sb-SnO_2/PbO_2 doped with and without the active particles were used as the anodes. The cathode was Pt sheet. At room temperature, the electrolyte was electrolyzed by constant current method with a current density of 20,000 A m^{-2}, and the cell voltage was recorded every 1 h until the voltage rose to higher than 10 V, indicating that the electrodes had deactivated.

RESULTS AND DISCUSSION

1. SEM Analysis

The SEM images of the electrodes surface are shown in Fig. 2. As can be seen from Fig. 2(a), the surface of the un-doped Ti/Sb-SnO_2/PbO_2 anode presents a typical pyramid structure. Fig. 2(b)-(d) shows the different magnifications of the anode surface of doped Ti/Sb-SnO_2/PbO_2. As can be seen from Fig. 2(b), the anode surface of doped Ti/Sb-SnO_2/PbO_2 belongs to a porous structure, and many pores can be seen on the surface, which is conducive to improving the specific surface area of the electrode and increasing the catalytic active site, thus improving the performance of the electrode [26]. Under a high-power scanning electron microscope, a series of Mn-Co_3O_4/CeO_2@C clusters (Fig. 2(c)) and dispersed particles (Fig. 2(d)) are seen to be loaded onto the surface and buried in the PbO_2 layer. At the same time, according to Fig. 2(a) and Fig. 2(c), it can be seen that compared with undoped Ti/Sb-SnO_2/PbO_2 anodes, the crystal shape of PbO_2 is clearer and the grain size is reduced after the addition of Mn-Co_3O_4/CeO_2@C, which also promotes the improvement of the catalytic performance [27]. The color intensity in EDS mapping (Fig. 2(e)) also confirms the deposition of Mn-Co_3O_4/CeO_2@C particles on the surface.

2. XRD Structural Characterization

It can be observed from the XRD pattern in Fig. 3(a) that there are both α-PbO_2 and β-PbO_2 characteristic peaks in the XRD pattern of the undoped PbO_2 anode. Comparing the XRD patterns of PbO_2 anodes with different Ce doping levels, it is found that the characteristic peak of α-PbO_2 is present in the XRD pattern of PbO_2 anodes without Ce doping, while the characteristic peak of β-PbO_2 is only observed in the XRD pattern of PbO_2 anodes with Ce doping. That indicates that doping of Ce transforms α-PbO_2 into β-PbO_2. It is thought that Ce doping may promote the crystal transition of PbO_2 [28]. In general, β-PbO_2 has a better electrocatalytic activity than α-PbO_2, so the doped electrode may exhibit an electrocatalytic performance [20,29]. Fig. 3(b) shows XRD patterns of Mn-Co_3O_4/CeO_2@C active particles, peaks of Co_3O_4 and CeO_2 are observed, respectively, in XRD pattern of Fig. 3(b) because Co_3O_4 with spinel structure and cubic CeO_2 cannot form mixed phase [30]. Note that no corresponding Mn oxide peak was found in the XRD pattern of Mn-Co_3O_4/CeO_2@C composite. Since the XRD peak of Co_3O_4 is very similar to that of $MnCo_2O_{4.5}$, it is speculated that Mn may be incorporated into the Co_3O_4 lattice, partially replacing the position of Co atom.

3. XPS Analysis

The elemental composition and valence state of the active particles were further studied by XPS spectra. As indicated in Fig. 4, XPS full spectra of all samples confirmed the presence of Mn, Co, Ce, C and O in the samples. The high-resolution spectra of Co 2p for all samples are depicted in Fig. 5(a). Peaks at 780.0 eV, 781.3 eV, 795.1 eV and 796.4 eV belong to Co^{3+} 2p3/2, Co^{2+} 2p3/2, Co^{3+} 2p1/2

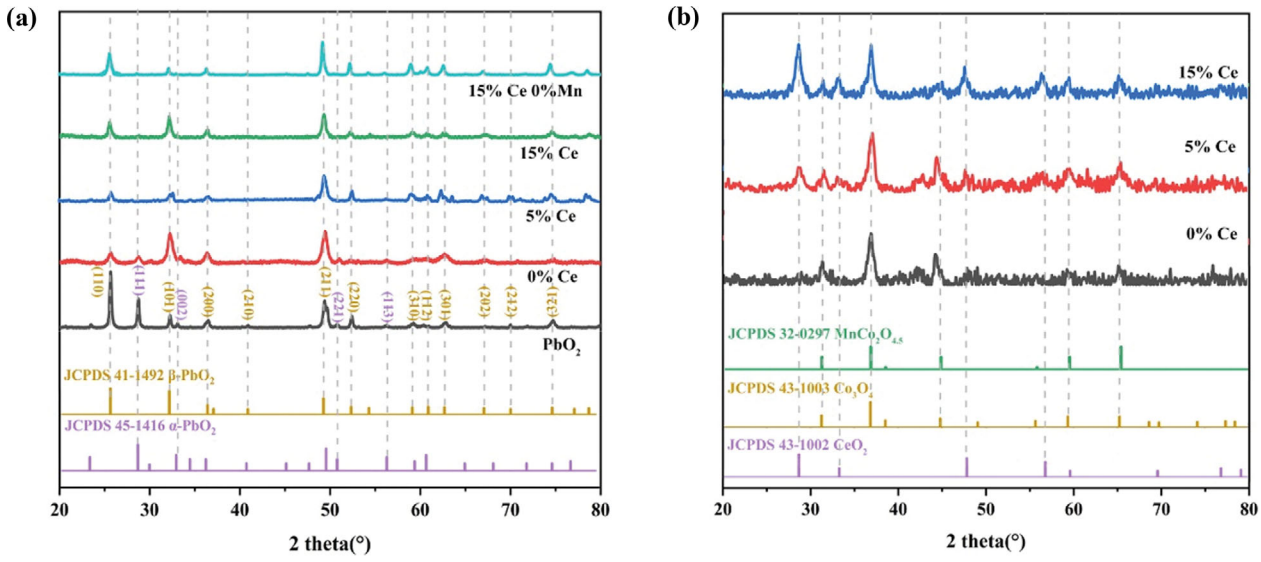

Fig. 3. XRD pattern: (a) Undoped and doped PbO_2 electrodes; (b) Mn-Co_3O_4/CeO_2@C active particles.

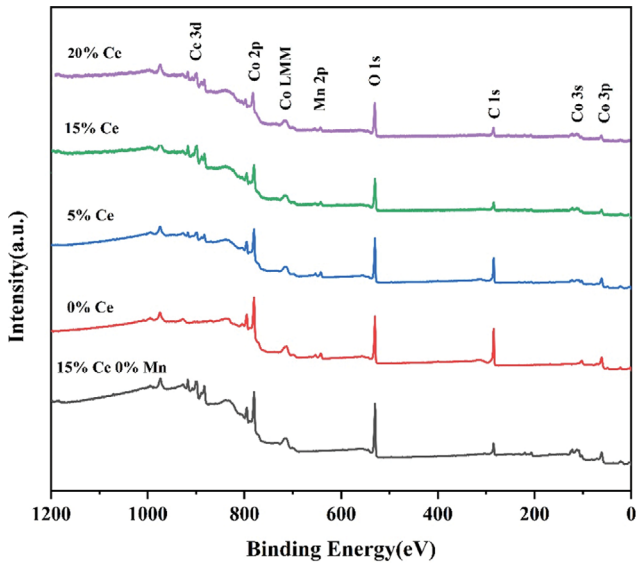

Fig. 4. The full spectrum of XPS high-resolution spectra analysis of Mn-Co_3O_4/CeO_2@C.

Table 1. The average valence state of active particles with different Ce content

Ce loading	Average valence state of Co	Average valence state of Mn
0% Ce	2.28	3.54
5% Ce	2.36	3.53
15% Ce	2.61	3.57

and Co^{2+} 2p1/2, respectively. Similarly, the signal of Mn can be divided into four peaks, which are located at 641.6 eV, 643.0 eV, 653.3 eV and 654.5 eV and correspond to Mn^{3+} 2p3/2, Mn^{4+} 2p3/2, Mn^{3+} 2p1/2 and Mn^{4+} 2p1/2, respectively. The XPS spectra of Ce correspond perfectly to the standard spectra of CeO_2, proving that Ce exists almost entirely in the form of CeO_2.

The average valence state of an element is obtained by the ratio of peak area of high-resolution spectra, as shown in Table 1. With the increase of Ce content, the oxidation state of Co in the active particles increased, while the oxidation state of Mn did not change significantly. The increase of Co oxidation state caused by Ce dop-

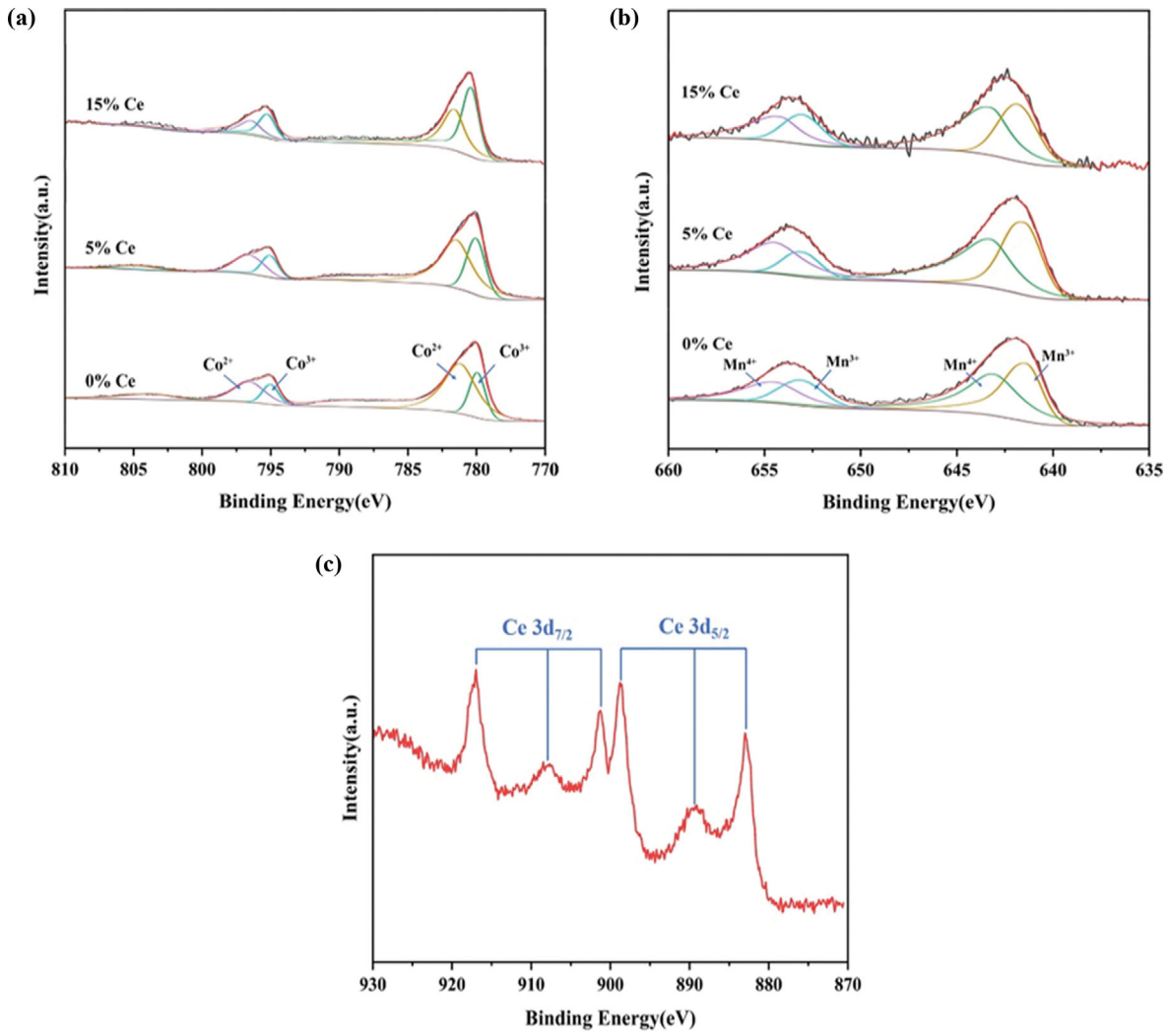

Fig. 5. The XPS high-resolution spectra analysis of Mn-Co_3O_4/CeO_2@C.

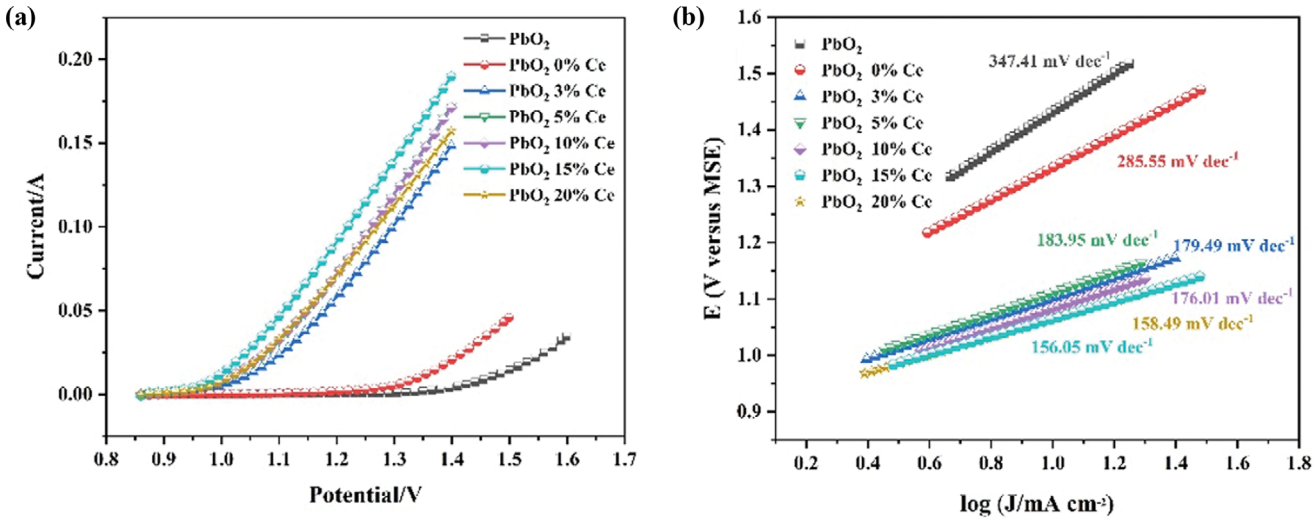

Fig. 6. The LSV curves and Tafel fitting plots for all electrodes: (a) the LSV curves, (b) Tafel fitting plots.

ing may be one of the reasons for the difference in electrochemical performance. When the doping amount of Ce is 15%, the average valence states of Mn and Co are 2.61 and 3.57, respectively. Combined with XRD and XPS results, Mn atom may replace part of Co atomic position in Co_3O_4 and exist in the form of $MnCo_2O_{4.5}$ [22].

4. Electrochemical Properties

The structural analysis of the active oxide composites indicated the formation of co-crystallization of Mn and Co oxides, which exhibited OER catalytic activity together. However, as mentioned above, CeO_2 is independent in the composite due to its crystal morphology, which is different from that of Co_3O_4. As an element commonly thought to help increase OER potential [32], the effect of different addition amounts of Ce in the active composite material on the electrochemical properties of a doped electrode has been studied.

LSV is used to test the OER performance of electrodes, as shown in Fig. 6(a). LSV curves of a series of PbO_2 anode materials were tested in 0.5 M H_2SO_4 solution at a scanning speed of 0.005 V s^{-1}. The test results show that the initial OER potential of PbO_2 electrode doped with active particles is generally lower in acidic electrolyte. When the Ce atoms doping rate is 15%, it has the best electrochemical performance. When the current density is 20 mA cm^{-2}, the potential is 1.027 V (vs. MSE), which is 508 mV lower than that of the undoped PbO_2 electrode (1.535 V vs. MSE). It was 370 mV lower than the doped PbO_2 electrode without Ce (1.397 V vs. MSE). When the current density increased gradually, the potential difference between the doped electrode and PbO_2 electrode increased gradually, indicating that Mn-Co_3O_4/CeO_2@C plays an important role in enhancing OER activity. Mn-Co_3O_4/CeO_2@C modified PbO_2 electrode has lower potential than PbO_2 electrode at the same current density, indicating that the addition of CeO_2 is conducive to OER occurrence. The Tafel equation (η=a+blogi, where η represents the overpotential, b is the Tafel slope, and a is the intercept) is used to fit the Tafel slope of different electrodes. The Tafel slope for a series of PbO_2 anodes has been labeled in Fig. 6(b). The lowest Tafel slope (156.05 mV dec^{-1}) occurs when the

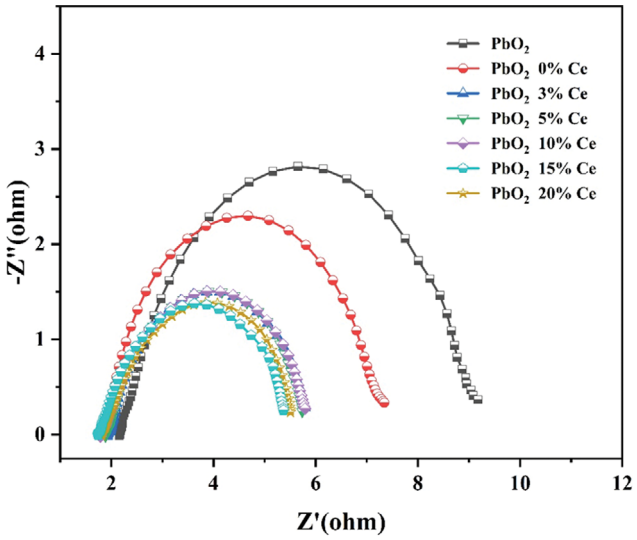

Fig. 7. EIS for all the anodes.

Ce atomic doping rate is 15%. A smaller Tafel slope means a lower activation energy for OER, which means a lower overpotential required to produce a given current density [33]. Interestingly, the OER catalytic capacity of CeO_2 is thought to be much lower than that of Co_3O_4 [31], However, when the two oxides were doped in Ti/Sb-SnO_2/PbO_2 anode, the OER activity of the electrode was enhanced, which was higher than that of the Co_3O_4 without Ce doped electrode.

OER kinetics was studied by EIS in 0.5 M H_2SO_4 solution with a fixed current density of 10 mA cm^{-2}. As shown in Fig. 7, the EIS spectrum shows a number of semicircles of different radii. The starting position of the semicircle can be used to compare the resistance values (R_s) of different electrodes. The small radius means that the electron transfer resistance (R_{ct}) is low in the OER process, leading to the improvement of the electrocatalytic activity of OER [34]. It can be observed from the figure that all doped active particle electrodes show similar resistance values and are slightly

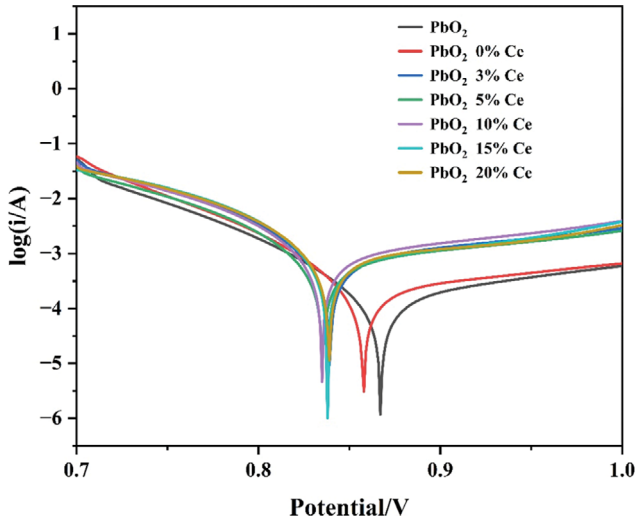

Fig. 8. Tafel polarization curves for all electrodes.

lower than PbO_2 electrodes, which is due to the improved conductivity caused by C doping, indicating that the doped electrodes have stable and reduced resistance. The electron transfer resistance R_{ct} of Mn-Co_3O_4/CeO_2@C doped PbO_2 electrode (3.64 ohm) is smaller than that of Mn-Co_3O_4@C doped PbO_2 electrode (5.31 ohm) and undoped PbO_2 electrode (6.91 ohm), which is consistent with the previous discussion, indicating that the charge transfer of the PbO_2 electrode doped with active particles is faster and the electrocatalytic activity of OER is enhanced. The co-doping of CeO_2 and Co_3O_4 can effectively reduce electron transfer resistance and promote OER reaction, which may be related to the interphase electron transfer between CeO_2 and Co_3O_4, and CeO_2 can promote the intrinsic oxygen evolution activity of Co_3O_4 [24,32,35].

The corrosion resistance of the electrodes was studied by Tafel polarization curve (Fig. 8). It can be seen that the Tafel polarization potential curves of all electrodes are in the range of 0.8-0.9 V, and the corrosion potential of the electrodes doped with Ce active particles is very similar to that of PbO_2 electrodes. From the point of view of corrosion current, the corrosion current of other electrodes is similar to that of PbO_2 electrode except the PbO_2 electrode mixed with 15% Ce, which has a slightly larger corrosion current. The above electrochemical results indicate that the co-doping of CeO_2 and Co_3O_4 can make the anode have stronger OER catalytic activity.

In order to demonstrate the effect of Mn and C addition on the electrochemical performance of electrodes, the Ti/PbO_2 electrode without Mn and C addition was used for electrochemical testing. As shown in Fig. 9, comparing an anode without Mn or C, the Mn-Co_3O_4/CeO_2@C modified PbO_2 electrode showed lower overpotential at the same current density, indicating that the addition of Mn and C is conducive to OER, and EIS showed that the addition of C could reduce R_s and R_{ct} and promote electron transfer.

5. Simulated Electrolytic Copper Experiment

In addition to OER electrocatalytic activity, stability is another key factor in evaluating copper electrodeposited electrodes. Ti/Sb-SnO_2/PbO_2 electrodes doped with active particles containing 15% Ce and the undoped PbO_2 electrodes were used to simulate copper electrodeposition. The stability of the electrodes was tested in 65 g L^{-1} Cu^{2+} and 150 g L^{-1} H_2SO_4 solution with current density of 20 mA cm^{-2} and electrodeposition temperature of 65 °C. The doped Ti/Sb-SnO_2/PbO_2 electrode is used for copper electrolysis with lower cell voltage about 400 mV than that of the un-doped Ti/Sb-SnO_2/PbO_2 electrode (Fig. 10).

In addition, the cell voltage decreased slightly at the initial stage of electrolysis and then remained stable and did not fluctuate significantly during the whole electrolysis process, indicating that the doped Ti/Sb-SnO_2/PbO_2 anode has good stability during copper electrodeposition. Fig. 11 shows that the electrode life of the Ti/Sb-SnO_2/PbO_2 anode doped with 15% Ce active particles reaches 72 h at the ultra-high current density (20,000 A m^{-2}), which is slightly higher than that of the Ti/Sb-SnO_2/PbO_2 anode without doping active particles. This indicates that the active materials coating anode prepared in this study has good catalytic activity as well as good corrosion resistance. The electrochemical properties of several anodes with different doped active ingredients in this study are compared

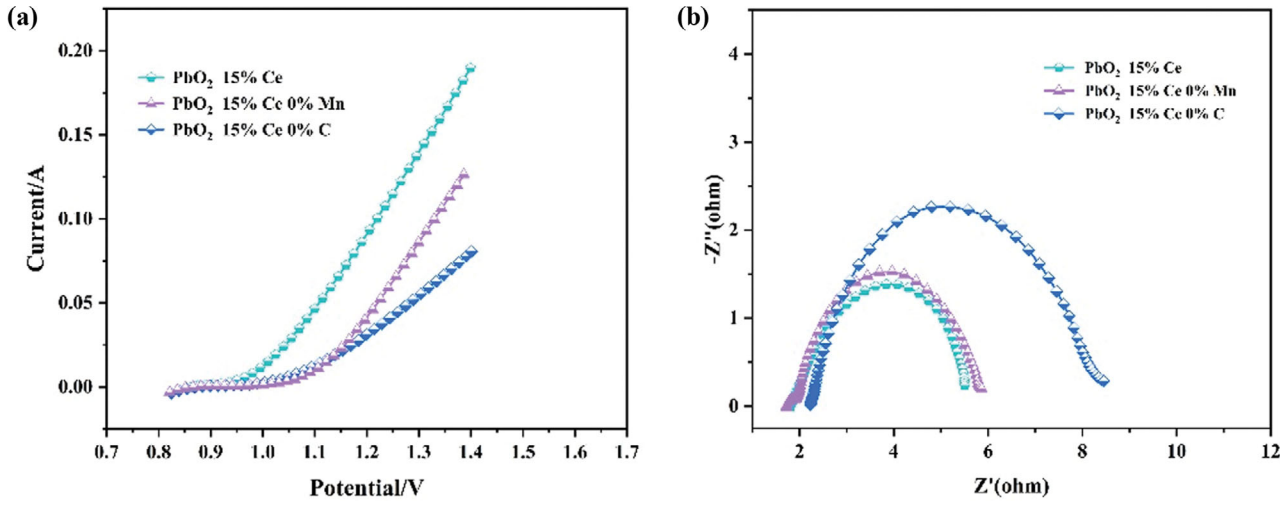

Fig. 9. Effect of Mn and C on the mechanical properties of electrodes.

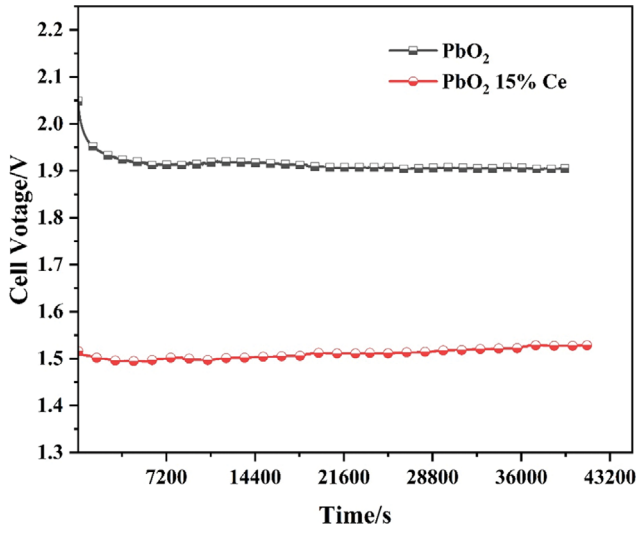

Fig. 10. Cell voltage of simulated electrodeposited copper experimental.

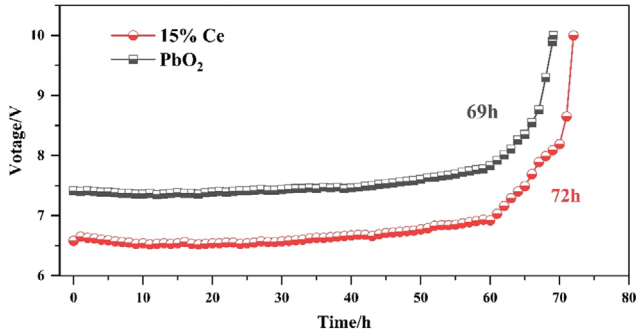

Fig. 11. Accelerated corrosion life test curve of undoped Ti/Sb-SnO_2/PbO_2 anode and Ti/Sb-SnO_2/PbO_2 anode doped with 15% Ce active particles.

and listed in Table 2.

CONCLUSION

Mn-Co_3O_4/CeO_2@C active particles were synthesized by pyrolysis and air annealing, and then electrodeposited on Ti/Sb-SnO_2 substrate with PbO_2 as exogenous particles. SEM and EDS characterization showed that Mn-Co_3O_4/CeO_2@C was embedded in the PbO_2 layer, which was beneficial for improving the electrocatalytic activity and stability. The obtained doped Ti/Sb-SnO_2/PbO_2 electrode containing 15% Ce had the best electrocatalytic activity, and the OER overpotential was only 453 mV when the current density was 20 mA cm^{-2}, which is 508 mV lower than that of the undoped Ti/Sb-SnO_2/PbO_2 electrode. In addition, the resulting modified Ti/Sb-SnO_2/PbO_2 electrode had stable activity, which remained stable for 12 h in simulated electrodeposition of copper. It also showed a relatively long service life, which lasted for about 72 h at the ultra-high current density of 20,000 A m^{-2}. This new type coated Ti anode is expected to be used in copper metallurgy to save energy consumption.

ACKNOWLEDGEMENTS

The authors are grateful for the financial support from the Shaanxi Science and Technology Department (2022GY-384, 2022JBGS2-07, 2021LLRH-05-21, S2022-YD-QFY-0107), the Open Foundation of Key Laboratory of Synthetic and Natural Functional Molecular Chemistry of Ministry of Education (KLSNFM2020001).

REFERENCES

1. L. Ding, J. Chen, T. Wang, J. Zhao, C. Chen and Y. Niu, *Miner. Eng.*, **135**, 21 (2019).
2. M. Stelter and H. Bombach, *Adv. Eng. Mater.*, **6**, 558 (2004).
3. Y. Liu, W. Zhu, Z. Chen, Q. Yu, Q. Hu, Z. Zheng, L. Gui and Y. Song, *Int. J. Hydrogen Energy*, **46**, 6380 (2021).
4. V. Krstić and B. Pešovski, *Hydrometallurgy*, **185**, 71 (2019).
5. L. C. Espinoza , P. Sepúlveda, A. García, D. M. d. Godoi and R. Salazar, *Chemosphere*, **251**, 126674 (2020).
6. H. W. Lim, D. K. Cho, J. H. Park, S. G. Ji, Y. J. Ahn, J. Y. Kim and C. W. Lee, *ACS Catal.*, **11**, 12423 (2021).
7. A. Touni, O. A. Grammenos, A. Banti, D. Karfaridis, C. Prochaska, D. Lambropoulou, E. Pavlidou and S. Sotiropoulos, *Electrochim. Acta*, **390**, 138866 (2021).
8. S. Pan, H. Li, D. Liu, R. Huang, X. Pan, D. Ren, J. Li, M. Shakouri, Q. Zhang, M. Wang, C. Wei, L. Mai, B. Zhang, Z. Wang, M. Graetzel and X. Zhang, *Nat. Commun.*, **13**, 2294 (2022).
9. C. Pasquini, I. Zaharieva, D. González-Flores, P. Chernev, M. R. Mohammadi, L. Guidoni, R. D. L. Smith and H. Dau, *J. Am. Chem. Soc.*, **141**, 2938 (2019).
10. X. Yang, H. Li, A. Lu, S. Min, Z. Idriss, M. N. Hedhili, K. Huang, H. Idriss and L. Li, *Nano Energy*, **25**, 42 (2016).

Table 2. Electrochemical data of different electrode samples

Anode	Overpotential (mV)	Tafel slope (mV dec^{-1})	R_s (ohm)	R_{ct} (ohm)	Accelerated life (h)
Undoped PbO_2	961	347.41	2.21	6.91	69
0% Ce	822	285.55	1.92	5.31	-
5% Ce	486	179.49	1.88	3.83	-
10% Ce	480	176.01	1.85	3.85	-
15% Ce	453	156.05	1.80	3.64	72
20% Ce	485	158.49	1.84	3.70	-

11. A. Li, S. Kong, C. Guo, H. Ooka, K. Adachi, D. Hashizume, Q. Jiang, H. Han, J. Xiao and R. Nakamura, *Nat. Catal.*, **5**, 109 (2022).
12. B. Chen, W. Yan, Y. He, H. Huang, H. Leng, Z. Guo and J. Liu, *J. Electrochem. Soc.*, **166**, 119 (2019).
13. X. Wang, L. Wang, D. Wu, D. Yuan, H. Ge and X. Wu, *Sci. Total Environ.*, **855**, 158880 (2023).
14. T. Lwai, M. Murakami, S. Takai, T. Yabutsuka and T. Yao, *J. Alloy Compd.*, **780**, 85 (2019).
15. K. Irikura, N. Bocchi, R. C. Rocha-Filho, S. R. Biaggio, J. Iniesta and V. Montiel, *J. Environ. Manage.*, **183**, 306 (2016).
16. S. Chen, B. Chen, S. Wang , W. Yan, Y. He, Z. Guo and R. Xu, *J. Alloy. Compd.*, **815**, 152551 (2020).
17. B. Yu, R. Xu, B. Chen, X. Wang and S. He, *Int. J. Hydrogen Energy*, **48**, 11131 (2023).
18. S. He, R. Xu, L. Sun, Y. Fan, Z. Zhao, H. Liu and H. Lv, *Hydrometallurgy*, **194**, 105357 (2020).
19. C. Zhang, J. Liu and B. Chen, *Ceram. Int.*, **44**, 19735 (2018).
20. X. Wang, J. Wang, W. Jiang, C. Chen, B. Yu and R. Xu, *Sep. Purif. Technol.*, **272**, 118916 (2021).
21. J. Wei, J. Wang, X. Wang, W. Jiang, N. Hu, L. Wang, M. Li, R. Xu and L. Yang, *Electrochim. Acta*, **432**, 141221 (2022).
22. X. Wang, J. Wang, B. Yu, W. Jiang, J. Wei, B. Chen, R. Xu and L. Yang, *J. Hazard. Mater.*, **428**, 128212 (2022).
23. C. Tang, Y. Lu, F. Wang , H. Niu, L. Yu and J. Xue, *Electrochim. Acta*, **331**, 165381 (2020).
24. Y. Liu, T. Sun, Q. Su, Y. Tang , X. Xu, M. Akram and B. Jiang, *J. Colloid Interface Sci.*, **575**, 254 (2020).
25. W. Alnoush, R. Black and D. Higgins, *Chem. Catal.*, **1**, 997 (2021).
26. Z. Zhao, Y. Long, S. Luo, Y. Luo, M. Chen and J. Ma, *J. Energy Chem.*, **60**, 546 (2021).
27. H. Kim, E. Hwang, H. Park, B. Lee, J. H. Jang, H. Kim, S. H. Ahn and S. Kim, *Appl. Catal. B-Environ.*, **206**, 608 (2017).
28. O. Shmychkova, T. Luk'yanenko, R. Amadelli and A. Velichenko, *J. Electroanal. Chem.*, **706**, 86 (2013).
29. H. Jin, X. Zhang, Y. Yu and X. Chen, *Chem. Eng. J.*, **435**, 135167 (2022).
30. Y. Liu, C. Ma, Q. Zhang, W. Wang, P. Pan, L. Gu, D. Xu, J. Bao and Z. Dai, *Adv. Mater.*, **31**, 1900062 (2019).
31. Z. Wei, X. Kang, S. Xu, X. Zhou, B. Jia and Q. Feng, *Chin. J. Chem. Eng.*, **32**, 191 (2021).
32. T. Shinagawa, A. T. Garcia-Esparza and K. Takanabe, *Sci. Rep.*, **5**, 13801 (2015).
33. C. C. L. McCrory, S. Jung, J. C. Peters and T. F. Jaramillo, *J. Am. Chem. Soc.*, **135**, 16977 (2013).
34. J. Huang, H. Sheng, R. D. Ross, J. Han, X. Wang, B. Song and S. Jin, *Nat. Commun.*, **12**, 3036 (2021).